

Non-invasive Placement and 3D Tracking of Myocardial Beads with SPAMM-tagged Magnetic Resonance Imaging

A Amini, P Radeva, M Elayyadi, W McBride, D Li, D Abendschein

CVIA Lab, Division of Cardiology, Washington University School of Medicine, St. Louis, USA

Abstract

In this paper, a specific Spatial Modulation of Magnetization (SPAMM) imaging protocol and associated image analysis methods are proposed. The imaging process creates long axis tag planes which are coincident with short-axis image slices at the time of on-set of tags. In addition, one set of short-axis tag planes are created coincident with long-axis image slices at the time of on-set of tags. Once short-axis and long-axis tag data synchronized with one another and with the EKG signal are obtained, the three sets of tag planes (two intersecting short-axis image slices and one intersecting long-axis image slices) are continuously reconstructed across several image slices for all temporal frames during the heart cycle with B-spline surfaces. Subsequently, a computer algorithm determines the intersection of these 3 sets of surfaces for a number of material points of the LV myocardium, allowing for visualization of 3D motion of these non-invasively placed beads during the entire cardiac cycle.

1. Introduction

Non-invasive techniques for assessing the dynamic behavior of the human heart are invaluable in the diagnosis of heart disease, as abnormalities in the myocardial motion sensitively reflect deficits in blood perfusion [10]. MRI is a non-invasive imaging technique that provides superb anatomic information with excellent spatial resolution and soft tissue contrast. Conventional MR studies of the heart provide accurate measures of global myocardial function, chamber volumes and ejection fractions, and regional wall motions and thickening. In MR tagging, the magnetization property of selective material points in the myocardium are altered in order to create tagged patterns within a deforming body such as the heart muscle.

The resulting pattern defines a time-varying curvilinear coordinate system on the tissue. During tissue contractions, the grid patterns move, allowing for visual tracking of the grid intersections over time. The intrinsic high spatial and temporal resolutions of such myocardial analysis schemes provide unsurpassed information about local contraction and deformation in the heart wall which can be used to derive local strain and deformation indices from different myocardial regions.

Several tagged imaging techniques have been proposed in the MR literature [10, 3]. The basic premise in all tagging schemes involves using a set of rf pulses to place tag planes in thin slices of the myocardium, perpendicular to the imaging plane which can then be tracked over the heart cycle. Physics of MR tagging as well as its application to the understanding of regional LV function are maturing and tagging is quite likely to play a major role in patient care in coming years. Fast imaging techniques also promise to provide the means for reducing the effect of tag relaxation which diminish image contrast in later phases of cardiac cycle. In order to handle the large magnitude of generated data, automated methods for analysis of sequences of tagged cardiac images will be a necessity. Several approaches to tagged MR image analysis have been proposed in the past. The distinguishing feature of the approach proposed in the present paper is direct computation of non-rigid motion of material points of the heart from SPAMM images using explicitly defined B-surface representations.

Previous work for analysis of SPAMM images includes [9, 7, 2, 1, 8, 4]. In comparison to these previous works, the present article provides machinery for very fast computation of tag surfaces using B-snakes on individual slices, does not require *a priori* computation of a solid, and furthermore since by design the surfaces are parametric, it leads to a naturally easy to implement algorithm for computing 3D material points.

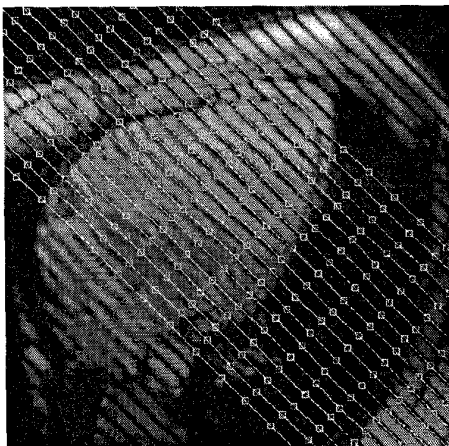


Figure 1: Position of short-axis image slices at the time of tag placement is drawn on a long-axis image acquired at the same time point in the heart cycle.

2. Imaging Protocol

A SPAMM pulse sequence was used to collect images of normal healthy volunteers. Multiple images in both short-axis and long axis views of the heart were collected to cover the entire volume without gaps. Immediately after the ECG trigger, rf tagging pulses were applied in two orthogonal directions. The repetition time (TR) of the imaging sequence was approximately 7.1 msec, the echo time (TE) was 2.9 msec, the rf pulse flip angle was 15 degrees, and the time extent of rf tag pulses was 22 msec. Echo sharing was used in collecting each time-varying image sequence for given slice position. Five data lines were collected for any time frame during each heart cycle, but two data lines were overlapped between two consecutive cardiac frames, resulting in an effective temporal resolution of approximately 22 msec. Other imaging parameters were: field of view = 330mm, data acquisition matrix size = 160×256 (phase encoding by readout), in-plane resolution = $2.1 \times 1.3\text{mm}^2$, slice thickness = 7mm, and tag spacing = 7mm. The total imaging time was therefore 32 heart beats for each Cine sequence, and the subject was instructed to breath only following each Cine acquisition. Since there were 19 volumetric temporal frames and 17 spatial slices in each image volume, all of the images were acquired in 544 heartbeats. In the long-axis view, there were also 19 temporal frames. However, 13 slices covered the entire heart in this case resulting in 416 heart beats of total imaging time.

The image orientations for the short-axis and long-axis views of the heart were first determined by col-

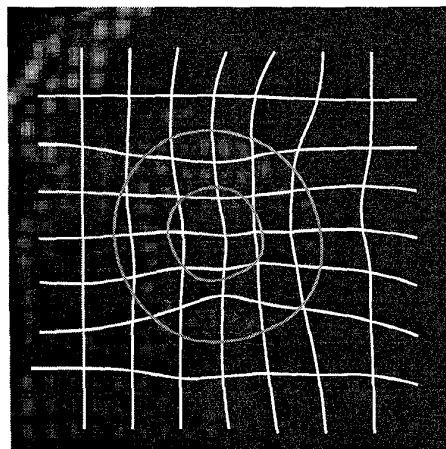


Figure 2: A grid of B-spline snakes on short-axis image slices in mid-systole. Note that for better illustration, in this figure as well as all analysis to follow every second tag line is utilized. The analysis area of interest is the region within the myocardial borders of the LV.

lecting multiple oblique angle scout images. For the short-axis images, one of the tagging planes was placed parallel to the long-axis imaging planes of the heart by manually setting the angles of the tagging plane in the coordinate system of the magnet to be the same as those of the long-axis view as determined from scout images. The coordinates of the center of the central tagging plane in the reference coordinates system (relative to the center of the magnet) were set to be the same as those of the center of one of the long-axis image planes to be acquired, again determined by the scout images. As a result, one set of tagging planes intersecting short-axis image slices coincided with long-axis images since both tag spacing and slice thickness were 7 mm center-to-center. The other short-axis tagging plane was placed orthogonal to the first tagging plane. Similarly, long-axis images were acquired with their tag planes coinciding with short-axis slice positions. Figure 1 displays position of the short-axis image slices on one long-axis image at end-diastole.

As a result of the imaging protocol outlined in this section, the tag intersections from short-axis images are the material points corresponding precisely to the intersection of three tag planes, and revealing for all time points in the cardiac cycle, 3D motion of these special points.

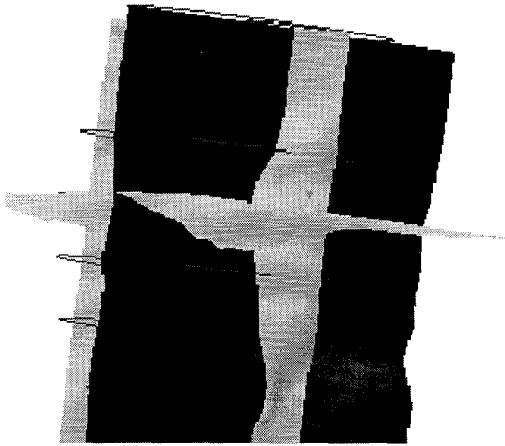


Figure 3: Figure illustrates the reconstruction of two orthogonal tag surfaces from a sequence of coupled B-spline curves in short-axis image slices (as in figure 1).

3. Computing time-dependent coordinates of material points

B-splines are suitable for representing a variety of industrial and anatomical shapes [6, 5, 1]. The advantages of B-spline representations are: (1) They are smooth, continuous parametric curves which can represent open or closed curves. For our application, due to parametric continuity, B-splines will allow for sub-pixel localization of tags, (2) B-splines are completely specified by few control points, and (3) Individual movement of control points will only affect their shape locally. In medical imaging, local tissue deformations can easily be captured by movement of individual control points without affecting static portions of the curve.

We use B-snakes to both track tag lines on short-axis and long-axis images and also to immediately generate B-spline surface representations from tag planes intersecting individual image slices. As an example, figures 2 and 3 illustrate the construction of intersecting cubic B-spline tag surfaces from a spatial stack of coupled B-snake grids from individual short-axis images.

As done in the case of coupled B-snakes of short-axis images, deformations of tag planes in the long-axis orientation are measured by creating B-spline surfaces from stacks of B-snakes on long-axis images. The difference between short-axis and long-axis image acquisitions is however that there is only one set of parallel tag planes intersecting long-axis images.

Coordinates of material points may be obtained

by computing intersections of three intersecting B-spline surfaces representing three intersecting tag surfaces. For each triplet of intersecting B-spline surfaces, $(S_1(u_1, v_1), S_2(u_2, v_2), S_3(u_3, v_3))$, the following computation is carried out

$$\min_{P_1, P_2, P_3} d^2(S_1, S_2) + d^2(S_1, S_3) + d^2(S_2, S_3) \quad (1)$$

where point P_i belongs to surface S_i and d is the Euclidean distance metric. The minimization is carried out using the method of Conjugate Gradient Descent which insures fast convergence of the method. Note that the overall distance function above can be written as

$$\begin{aligned} & \|S_1(u_1, v_1) - S_2(u_2, v_2)\|^2 + \\ & \|S_2(u_2, v_2) - S_3(u_3, v_3)\|^2 + \\ & \|S_1(u_1, v_1) - S_3(u_3, v_3)\|^2 \end{aligned} \quad (2)$$

with the goal of finding the parameters (u_i, v_i) for the triplet of surfaces. The computed parameters will in fact be surface parameters of the intersection point. For the iterative optimization process, a good initial set of parameters has been found to be parameters of the intersection point assuming linear B-spline bases. The algorithm was tested on an image sequence which included 17 slices and 19 frames (17×19 images) yielding temporal position of around 250 material points over the heart cycle. In a movie of these material points, the 3D motion of individual SPAMM points of the myocardium is clearly apparent.

Figure 4 displays results of the intersection computation for few of the material points.

4. Conclusions

In conclusion, we have described efficient methods for visualization and tracking of 3D material points of the heart from 2 sets of orthogonal tagged MR views. We have argued that in comparison to other forms of tag representation, use of B-splines has several advantages, including immediate generation of tag surfaces, subpixel accuracy for tag plane localization and parametric continuity, as well as the need to only assign the location of few control points in order to determine the location of a complete tag plane. Currently, the system is being used in actual clinical situations as part of a large clinical study.

Acknowledgements

This work is supported in part by a grant from Whitaker Biomedical Engineering Foundation, and

grant 1R29HL57628 from the National Institutes of Health.

References

- [1] A. A. Amini, R. W. Curwen, and J. C. Gore. Snakes and splines for tracking non-rigid heart motion. In *European Conference on Computer Vision*, pages 251–261, University of Cambridge, UK, April 1996.
- [2] A. A. Amini and et al. Energy-minimizing deformable grids for tracking tagged MR cardiac images. In *Computers in Cardiology*, pages 651–654, 1992.
- [3] L. Axel and L. Dougherty. MR imaging of motion with spatial modulation of magnetization. *Radiology*, 171(3):841–845, 1989.
- [4] W. Kerwin and J. Prince. Generating 3-D cardiac material markers using tagged mri. In *Information Processing in Medical Imaging (IPMI)*, pages 313–326, 1997.
- [5] S. Menet, P. Saint-Marc, and G. Medioni. B-snakes: Implementation and application to stereo. In *Proceedings of the DARPA Image Understanding Workshop, Pittsburgh, PA*, pages 720–726, Sept. 1990.
- [6] M. E. Mortenson. *Geometric Modeling*. John Wiley and Sons, New York, 1985.
- [7] J. Park, D. Metaxas, and L. Axel. Volumetric deformable models with parameter functions: A new approach to the 3d motion analysis of the LV from MRI-SPAMM. In *International Conference on Computer Vision*, pages 700–705, 1995.
- [8] P. Radeva, A. Amini, and J. Huang. Deformable B-Solids and implicit snakes for 3D localization and tracking of SPAMM MRI data. *Computer Vision and Image Understanding*, 66(2):163–178, May 1997.
- [9] A. Young, D. Kraitchman, L. Dougherty, and L. Axel. Tracking and finite element analysis of stripe deformation in magnetic resonance tagging. *IEEE Transactions on Medical Imaging*, 14(3):413–421, September 1995.
- [10] E. Zerhouni, D. Parish, W. Rogers, A. Yang, and E. Shapiro. Human heart: Tagging with MR imaging – a method for noninvasive assessment of myocardial motion. *Radiology*, 169:59–63, 1988.

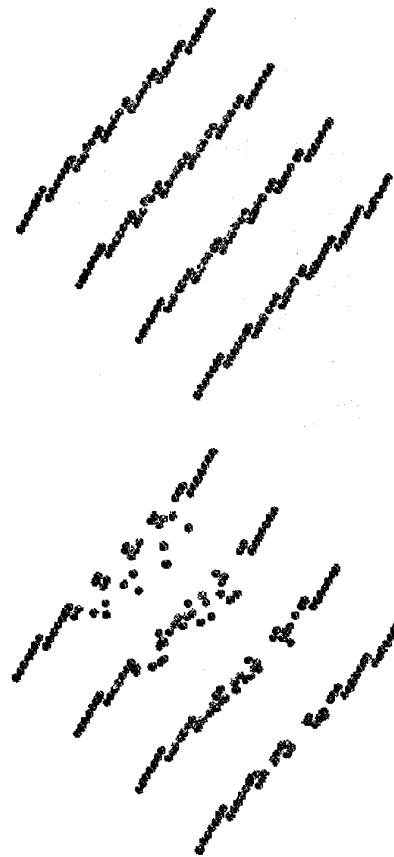


Figure 4: Initial 3D location of material points shown on every fourth slice of MRI data is displayed on the top. New computed location of material points one-third through systole is shown in the bottom. Non-rigid motion of material points of the heart can be appreciated: points further up in slices (around the base) move downwards, whereas points near the heart's apex are relatively stationary.

Address for correspondence.

Amir Amini, Ph.D.
CVIA Laboratory
Box 8086, 660 S. Euclid Ave.
Washington University Medical Center
St. Louis, MO 63110